Angle-dependent study of a direct optical transition in the *sp* bands of Ag(111) by one- and two-photon photoemission

Aimo Winkelmann,[1,2] Vahit Sametoglu,[2] Jin Zhao,[2] Atsushi Kubo,[3,2] and Hrvoje Petek[2,*]

[1]*Max-Planck-Institut für Mikrostrukturphysik, Weinberg 2, D-06120 Halle, Germany*
[2]*Department of Physics and Astronomy, University of Pittsburgh, Pittsburgh, Pennsylvania 15260, USA*
[3]*PRESTO, Japan Science and Technology Agency, 4-1-8 Honcho Kawaguchi, Saitama 332-0012, Japan*

We have measured angle-dependent photoemission spectra for one-photon and two-photon excitation from Ag(111). The observed dispersion of the *sp*-band transition of Ag(111) can be reproduced using a nearly-free-electron model for the initial and final states involved. The observed dispersion agrees with the known band structure. We illustrate how the strong refraction of low-energy electrons becomes a limiting factor to obtain quantitative band-structure information. Conversely, low-energy electrons of a well-defined direct optical interband transition can provide a sensitive probe of the inner potential. We observe asymmetric two-photon photoelectron intensity distributions with respect to detection along the surface normal. These intensity distributions can be well described by a phenomenological model which employs the Fresnel equations to calculate the electric field components of the incident radiation inside the sample. Very good agreement is found using tabulated optical constants and a momentum matrix element, which is oriented along the surface normal. In contrast, the observed intensity distribution for one-photon photoemission from Ag(111) does not fit the simple Fresnel model. We interpret this as the influence of surface photoemission. By comparison to Cu(001), we show that the expected intensity distributions of the Fresnel model for one-photon photoemission and two-photon photoemission are valid for an orientation of the momentum matrix element along the surface normal if the influence of additional effects like surface photoemission can be neglected.

I. INTRODUCTION

Angle-resolved photoemission spectroscopy (ARPES) is a powerful and general tool to investigate the energy-momentum dispersions of the electronic states, which define the band structure of solids. A wealth of knowledge about the initial and final states involved in the photoexcitation process has been obtained using this method.[1] In ARPES, by considerations based on energy and momentum conservation, peaks in the photoelectron energy spectrum can be ascribed to transitions between the occupied and unoccupied states separated by the energy of a single photon of the exciting radiation (one-photon photoemission, 1PPE). Using tunable synchrotron radiation and a fixed geometry with angle-resolved electron detection along the surface normal, a sampling of the band structure along a high symmetry direction in reciprocal space is conceptually simplified. It is also possible to obtain band-structure information by taking angle-dependent photoemission spectra at fixed photon energy in symmetry planes[2] or even the whole hemisphere above the sample.[3] The interpretation of such experiments, however, is more involved because of the more complicated form of the sampled regions in reciprocal space due to the nonconservation of the perpendicular component of the wave vectors. In all these types of measurements, information about the electronic band structure can be gained, first of all, by the analysis of the observed dispersion of peak *positions* in the photoelectron spectrum. To access the information contained in the photoemitted *intensities* is more complicated, because, in the general case, this has to involve comparison with calculated photoelectron spectra.[4]

With the application of high-power ultrafast laser systems, it also became possible to observe two-photon photoemission

(2PPE), where the initial state electrons are excited by the energy of two photons instead of only single photons as is the case in ARPES.[5,6] In the two-photon photoemission process, intermediate unoccupied states above the Fermi energy are involved. One of the main successes of 2PPE is to observe the energy- and momentum-dependent dynamics of excited electrons in these intermediate states directly in the time domain by using a pump-probe configuration.[7] Experimentally, the application of 2PPE is usually limited to photon energies where no one-photon photoemission can occur because this would overwhelm the 2PPE signal. However, apart from this limitation, the basic mechanisms governing both angle-resolved coherent 2PPE and ARPES are expected to be closely related.

As a model system for the quantitative analysis of photoemission spectra, the bulk band structure of silver has been extensively studied by 1PPE ARPES.[8–10] The importance of the polarization of the incident light on the distibution of the photoemitted electrons was studied experimentally and theoretically,[11–13] and the importance of the momentum matrix elements for the observed intensities of energy-dependent transitions was shown.[14] Spin-resolved measurements in combination with relativistic one-step photoemission calculations for Ag(111) have been used to compare different approximations for the exchange-correlation potential.[15] The Shockley surface state on Ag(111) was also investigated by ARPES.[16–20] The ARPES results have been analyzed using several theoretical bulk band-structure calculations.[21–23] Recently, the bulk valence band structure of silver has been investigated by hard x-ray photoemission spectroscopy.[24] In a photon energy range relevant to our investigation, significant interference between surface and bulk
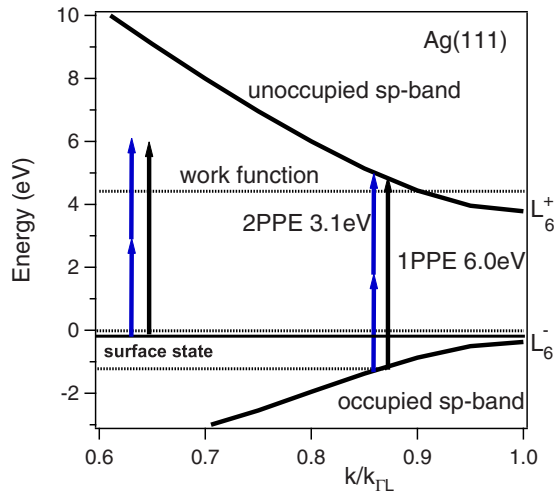
FIG. 1. (Color online) Bulk band structure along the ΓL line relevant for normal emission Ag(111), with indicated direct optical transitions between occupied and unoccupied *sp* bands by 2PPE and 1PPE. Also shown is the position of the occupied Shockley surface state at -65 meV, which is excited to a free-electron final state.

photoemission has been observed for Ag(111),[25,26] and the influence of collective surface plasmon excitations on the angle- and energy-resolved photoyields was studied.[27]

The 2PPE studies involving Ag(111) have mainly focused on the observation of image-potential states and their relaxation dynamics.[28–30] Concerning direct optical bulk transitions, it was shown that a systematic comparison of 1PPE and 2PPE measurements can be used to differentiate between surface states and bulk contributions.[31] An analysis of near-threshold two-photon electron emission from smooth and rough polycrystalline silver films has been given on the basis of a two-orthogonalized-plane-wave model for the involved *sp* bands.[32]

In a previous study, it was shown how the 2PPE spectrum of Ag(111) at $\hbar\omega=3.1$ eV can be simulated using optical Bloch equations and a nearly-free-electron model for the band structure.[33] In this contribution, we will present results of angle-dependent 2PPE and 1PPE measurements from the Ag(111) surface. Specifically, we will look at the effects observed when a transition between occupied and unoccupied *sp* bands is excited either by single photons (1PPE) or by simultaneous excitation by two photons (2PPE) of nearly half the energy used for 1PPE. For electrons emitted in the direction of the surface normal, the corresponding band structure is shown in Fig. 1. It will be shown that based on the observed dispersion, the direct optical transition from occupied to unoccupied *sp*-bulk bands agrees with the theoretically expected dispersion obtained from a nearly-free-electron band-structure model. The observed dispersion of this transition is very similar for 1PPE and 2PPE measurements on the Ag(111) surface. The intensity variation observed in the angle-dependent 2PPE spectra can be well explained by the application of the Fresnel equations of classical optics. From this model, we expect characteristic differences between the angular intensity variations in 1PPE and 2PPE, which should be almost independent of the spe-

cific substrate and photon energy used if additional influences like surface photoemission are negligible. This is shown by comparison with measurements on Cu(001). In contrast, the 1PPE intensity from Ag(111) does not fit a simple Fresnel model and seems to be strongly influenced by interference from surface photoemission.

Additionally, we suggest that the strong refraction effect of the very low kinetic energy photoelectrons at off-normal detection is a sensitive probe to gain insight into the behavior of the inner potential, which is not exactly known at these energies and which is expected to be strongly influenced by exchange and correlation effects.[34] At the same time, knowledge of the potential at the surface is crucial for the interpretation of imaging techniques using low-energy electrons and for the understanding of the chemical reactivity of surfaces.

The structure of the paper is as follows: after specifying the experimental details, we will extract from the general features of photoemission theory a phenomenological model which takes into account the most relevant angular dependencies. Then we will apply this model for the analysis of the experimental data. We will also discuss the implications of our findings for the mapping of electronic structure by angle-resolved 2PPE.

II. EXPERIMENTAL DETAILS AND RESULTS

For the photoemission measurements, a commercial Ag(111) crystal was prepared by standard techniques of multiple, sequential cycles of Ar^+-ion sputtering and annealing under UHV conditions. The sample surface quality was checked by the quality of the photoemission spectra converging to minimum inelastic background and maximum work function.

The photoemission light source is a self-made Ti:sapphire oscillator with chirped mirrors for dispersion compensation operating at 90 MHz repetition rate. For the two-photon photoemission measurements, second harmonic pulses are generated from the fundamental in an 80 μm β-BaB$_2$O$_4$ (BBO) crystal (3.1 eV photon energy, 200 meV bandwidth, and 10 fs pulse length). Additionally, one-photon photoemission spectra were measured with the fourth harmonic of the Ti:sapphire laser, which is generated by subsequent frequency doubling of the second harmonic.

The angle-resolved photoemission spectra are recorded under UHV conditions (10^{-10} mbar) at 100 K sample temperature by a commercial hemispherical electron analyzer (OMICRON EA125) with an angular resolution of 0.5° and an energy resolution of 40 meV. For the measurements, the sample was biased at -2 V. At the UHV chamber, the angle of the *p*-polarized incident light and the direction of the electron analyzer are fixed to 45°, leading to a simultaneous change in incidence and emission angles when the sample is rotated along an axis perpendicular to the optical plane for angle-dependent measurements (see Fig. 2).

In Fig. 3, we show an angle-dependent measurement of 2PPE and 1PPE spectra from Ag(111) for *p*-polarized incident light. The spectral features due to the *sp*-band transition and the surface state are clearly discernable. The surface state has dispersed above the Fermi level for detection angles
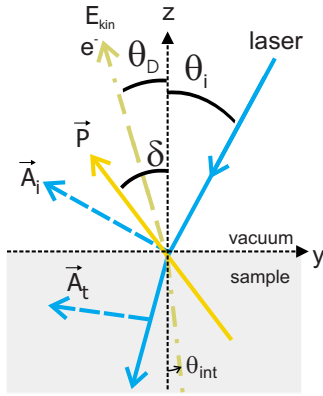
FIG. 2. (Color online) Geometry used for angle-dependent measurements. The direction between incident light and detected electrons is fixed to $\theta_i = 45° + \theta_D$. The direction of the photoemitted electron inside the sample is θ_{int}. Incident and refracted vector potentials $\vec{A}_i$ and $\vec{A}_t$. Momentum matrix element $\vec{P}$, characterized by the angle δ.

larger than 10°, while the *sp*-band transition can be seen in the whole observed energy range. The 2PPE intensity is clearly asymmetric with respect to the surface normal, while the 1PPE intensity looks more symmetric. The increased intensity of the surface state relative to the *sp*-band transition in 1PPE with respect to 2PPE is caused by a stronger surface photoemission component and, to a lesser extent, the decreased spectral width of the 6.0 eV pulses, which is due to the phase matching limits of the BBO crystal.

From the width of the observed spectra at normal emission, the work function can be deduced as 4.5 eV in accordance with previous studies.[26,28]
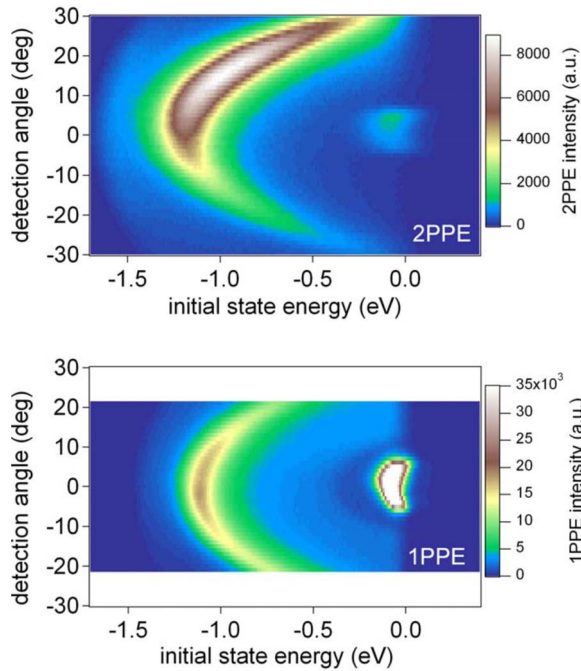

FIG. 3. (Color online) Experimentally measured intensities from Ag(111) by 2PPE ($\hbar\omega = 3.1$ eV) and 1PPE ($\hbar\omega = 6.0$ eV). Intensity scales are indicated.
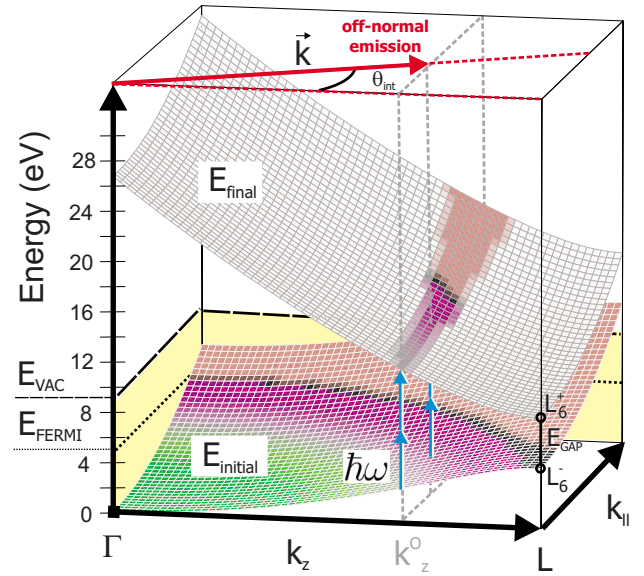

FIG. 4. (Color online) Nearly-free-electron band structure for initial and final *sp* states involved in the direct optical two-photon transition on Ag(111). Initial states which can be directly excited have been mapped onto the final state band. Only states up to the Fermi energy (black border) are occupied. The emitted direction is changed from θ_{int} by refraction when the photoelectron escapes the sample.

III. THEORETICAL MODELING OF PHOTOEMISSION

A. Dispersion

We first need to explain the observed change in the peak position of the *sp*-band transition when changing the direction of the detected outgoing electrons. To accomplish this, we model the relevant initial and final state band structures to define the curve of constant energy difference that shows where the incident radiation can induce direct optical transitions between these states.[35]

The *sp* bands relevant for our observed transitions are well described by a nearly-free-electron (NFE) model taking into account two orthogonalized plane waves (OPW).[36] We show the initial and final *sp*-band states near the Γ-L line calculated using this approximation in Fig. 4. The 2-OPW NFE model implies rotational symmetry around the Γ-L line. The size of the gap between L_6^- and L_6^+ is taken to be 4.2 eV, with L_6^- located −0.3 eV below the Fermi energy.[9] The band bottom is at 9.5 eV below the vacuum level.

The direct optical transition will take place in a region of k space where the difference between initial and final states is equal to the photon energy for 1PPE or to two times the photon energy in 2PPE. In this way, the perpendicular and parallel components of the $\vec{k}$ vectors taking part in the transition and, thus, the internal angle θ_{int} of $\vec{k}$ with respect to the surface normal in the $\langle 111 \rangle$ direction are determined. In the 2-OPW NFE model, these transitions take place at *fixed* k_z along Γ-L and varying parallel momentum $k_\parallel$ (Fig. 4). This is a special feature of the free (1-OPW) and nearly free (2-OPW) electron models. For a more general band structure, the curves of constant energy difference are more complicated.

To describe the refraction of the photoelectrons, we assume that a potential step $V_R > 0$ has to be overcome when crossing the sample-vacuum barrier. In the NFE model, this energy corresponds to the height E_{vac} of the vacuum level above the band bottom. As the kinetic energies are measured with respect to the vacuum level, the electrons inside the sample will have an energy of $E_{kin} + V_R$. This will have the effect that electrons emitted at the angle θ_{int} inside the sample will be detected at the angle θ_D in vacuum:

$$\frac{\sin \theta_D}{\sin \theta_{int}} = \sqrt{\frac{E_{kin} + V_R}{E_{kin}}}. \tag{1}$$

By using this simplified model, the dispersion of the direct *sp* transition is determined by a small number of parameters: the gap size $E_{gap} = 2V_{111}$, with V_{111} the pseudopotential Fourier component of the reciprocal lattice vector $\vec{G} = (\bar{1}, \bar{1}, \bar{1})$, the position of vacuum E_{vac}, and the Fermi energy E_{Fermi} (Fig. 4), with the work function $\Phi = E_{vac} - E_{Fermi}$. Furthermore, in the NFE model, the momentum matrix element has the simple form[37] of $\vec{P}_{if} \propto \vec{G}$, which will be relevant for the analysis of the observed intensities. Of course, we can expect this model to be valid only for a limited range of parallel momenta $k_\parallel$ beyond which the band structure will start to deviate from the simple NFE model assumed here.

B. Photoemitted intensity

By using first order perturbation theory to describe the interaction of the electromagnetic field with the sample atoms,[1,38] a Fermi golden rule expression for the photocurrent $I(f)$ from an initial wave function ψ_i emitted into the final state gives

$$I(f)^{1PPE} \propto |\langle \psi_f | V_I | \psi_i \rangle|^2 \delta(E_f - E_i - \hbar\omega)$$
$$= |M_{if}|^2 \delta(E_f - E_i - \hbar\omega), \tag{2}$$

where ψ_f is the final state wave function in the form of a time-reversed low-energy electron diffraction (LEED) state, and V_I is the interaction potential due to the incident radiation:

$$V_I = \frac{-e}{2mc} [\vec{A} \cdot \vec{p} + \vec{p} \cdot \vec{A}]. \tag{3}$$

Only terms linear in $\vec{A}$ are considered. The matrix element between initial and final states can be written as

$$M_{if} = \frac{ie\hbar}{2mc} \langle \psi_f | \vec{A}(\vec{r}) \cdot \nabla | \psi_i \rangle = \vec{A} \cdot \vec{P}_{if}, \tag{4}$$

where $\vec{P}_{if}$ is called the momentum matrix element. The Coulomb gauge $\nabla \cdot \vec{A} = 0$ has been applied, which, however, is valid only in the bulk. At the surface, the nonvanishing $\nabla \cdot \vec{A}$ term will cause an additional coherent contribution which is usually termed surface photoemission and which we think is relevant for the 1PPE measurements from Ag(111) (see below).

The two-photon photoemission intensity is obtained from second order time-dependent perturbation theory as a sum involving all possible intermediate states[39,40] m:

$$I(f)^{2PPE} \propto \left| \sum_m \frac{\langle \psi_f | V_I | \psi_m \rangle \langle \psi_m | V_I | \psi_i \rangle}{E_m - E_i - \hbar\omega} \right|^2 \delta(E_f - E_i - 2\hbar\omega). \tag{5}$$

For the observed transition in Ag(111), there are no resonant intermediate states. For this case of nonresonant excitation in a nearly-free-electron two-band model, the square of the product of the matrix elements in Eq. (5) can be shown[32] to depend as $|M_{fm} M_{mi}^\star|^2 \propto \cos^4 \Theta$ on the angle Θ between $\vec{A}$ and $\vec{p}$, so that we write the photoemission intensity with an effective momentum matrix element $\vec{P}_{eff}$:

$$I(f)^{2PPE} \propto |\vec{A} \cdot \vec{P}_{eff}|^4. \tag{6}$$

The observed angle-dependent intensities can now be thought of as originating from two main types of contributions. Firstly, there are angle-dependent changes of the electric field vector in the surface region due to the change in the angle of incidence of the laser radiation. In traditional optics, this is described by the Fresnel equations, which quantify how the magnitude and the direction of the incident vector potential as well as the relative phase between the *s* and *p* polarization components will change when entering the metal. This is described by complex amplitude reflection and transmission coefficients.[41] Secondly, the coupling of this incident polarization to the electron system will lead to an angle-dependent probability of detecting the excited electrons in the direction specified by the analyzer.

If one is only interested in the total yield of photoelectrons, irrespective of their emission direction, the total energy deposited in the sample should be relevant. This will be proportional to $(1 - R_{p(s)})^n$, where $R_{p(s)}$ is the reflectivity of the sample for $p(s)$-polarized incident light and n is the order of the photoemission process. For p-polarized light, increased photoemission should occur near the pseudo-Brewster angle, where the reflectivity is minimized and more intensity is transmitted into the sample. Good agreement with these expectations has been shown in multiphoton photoemission experiments from tungsten and copper.[42]

For angle-resolved photoemission, the transition matrix element is governed to a large extent by the relative orientation of the vector potential $\vec{A}_t$ and the photoelectron momentum $\vec{p}$, as can be seen from Eq. (3). These effects are separated in Eq. (4) into the vector potential $\vec{A}_t$ and the momentum matrix element $\vec{P}_{if}$, which depends on the angle of the emitted final state electron. In our experiment, this angle is in a fixed relation to the incidence angle of the laser. We will show below that the variation in the z component of $\vec{A}_t$ (Fig. 2) is the most relevant contribution for p-polarized incident light.

A nonvanishing $\nabla \cdot \vec{A}$ term due to the symmetry breaking by the surface will provide an additional coherent channel by which initial and final states can be coupled. Because the $\nabla \cdot \vec{A}$ term is only relevant in a very narrow spatial region near the surface, this part of the interaction potential provides Fourier components of a broad spectrum of crystal mo-

mentum. This means that initial and final states of different crystal momenta will be coupled, and the condition of vertical optical transitions in the reduced zone scheme is relaxed.

The simplest model to account for the $\nabla \cdot \vec{A}$ term at the surface is a step dielectric function which leads to a contribution $dA_\perp(z)/dz$ proportional to $[\epsilon(\omega)-1]\delta(z)$, where in the real situation the delta function is broadened. The contribution of surface photoemission to the matrix element was estimated as[26,43]

$$M_{if} \propto \vec{A}_t \cdot \vec{P}_{if} + \Delta A_z \frac{C}{2d} \equiv \vec{A}_t \cdot \vec{P}_{if} + M_S(\vec{A}_i, \epsilon(\omega), C_S), \quad (7)$$

with the change of the z component of $\vec{A}$ when going from vacuum into the sample over an effective thickness d:

$$\Delta A_z = |\vec{A}_i| \left(\frac{2\cos\theta_i \sin\theta_i}{\epsilon\cos\theta_i + \sqrt{\epsilon - \sin^2\theta_i}} - \sin\theta_i \right) \quad (8)$$

for the incident vector potential $\vec{A}_i$. If this model is assumed, an additional complex fit parameter $C_S = C/2d$ enters into the description of the angle-dependent intensities.

Several other processes are present which might influence the angular dependence of the photoemitted intensity. For instance, more of the excited photoelectrons from a certain depth will be scattered inelastically when they have to travel longer inside the material at larger exit angles. The electrons which are left and approach the solid-vacuum barrier from inside the sample within a certain solid angle are refracted into a larger solid angle in vacuum. This again reduces the intensity at larger exit angle in a symmetric way like the inelastic losses. Also, the observed peak shapes will be changed due to the varying $\vec{k}$-space resolution with exit angle. All these effects will be most pronounced at exit angles typically larger than 30°, and will be symmetric as a function of the emission angle with respect to the surface normal. Thus, if they are relevant, they are expected to reduce any asymmetry that is present rather than be a cause of it.

1. Electromagnetic field at the surface

At the solid-vacuum interface, the incident light is subject to refraction. This causes the vector potential inside the sample to be different than in vacuum. We will assume in our model that the Fresnel equations[44,45] can be used to give the components of the transmitted vector potential $\vec{A}_t$ as a function of the incident vector potential $\vec{A}_i$ and the dielectric function of the substrate $\epsilon(\omega)$:

$$\vec{A}_t = \vec{A}_t(\vec{A}_i(\theta_i), \epsilon(\omega)). \quad (9)$$

If the dipole matrix element for the observed transition is directed along the surface normal, the photoemitted intensity is governed by the A_z component of the vector potential. This is given by[44,45]

$$\frac{A_z}{A_0} = \frac{2\cos\theta_i \sin\theta_i}{\epsilon\cos\theta_i + \sqrt{\epsilon - \sin^2\theta_i}}. \quad (10)$$

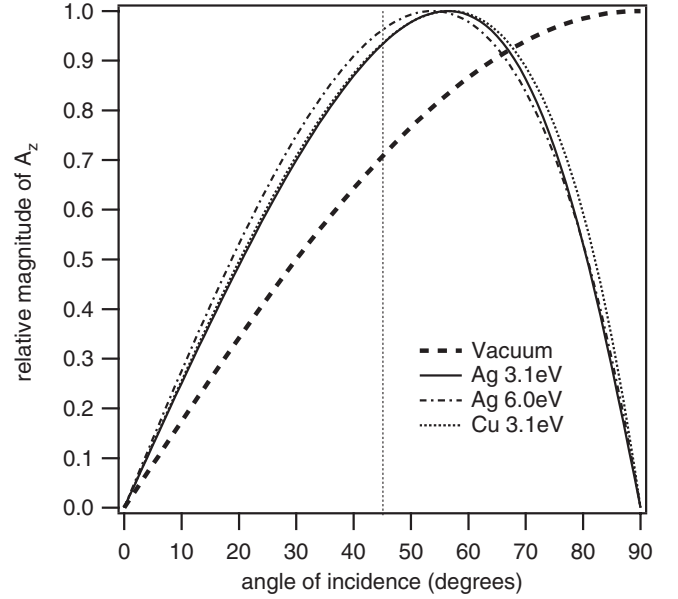In Fig. 5, it can be seen that the angular variation of the A_z

FIG. 5. Relative variation of the magnitude of the A_z component of the field inside the substrate for different photon energies and materials.

component is almost independent of the photon energy and whether we look at silver or copper. This behavior applies to a large selection of materials and photon energies used in angle-resolved photoemission, as can be seen, for instance, in Ref. 45. This means that our results will be of general significance for the comparison of angle-dependent linear and nonlinear photoemission experiments in our type of setup because, obviously, the optical properties at the surface do not have to be known very exactly.

We have to stress here that our treatment will be valid only if the observed transition can be assumed to take place inside the bulk, where the refracted electromagnetic field is relevant. The situation will become more difficult to treat if one is interested in transitions involving surface states, where there is interference of reflected and refracted radiations and where the influence of boundary effects of the electromagnetic field and of collective excitations like surface plasmons is most pronounced. In the general case, for arbitrary direction of the momentum matrix element, one has to include, of course, all components of the electromagnetic field in the analysis. Also, for the analysis of photoemission from *adsorbed* species, the field just *outside* the surface is relevant. Approaches to describe the corresponding electric fields are known from surface infrared spectroscopy.[46] For the case of 2PPE, angle-dependent measurements then allow conclusions about the direction of the dipole matrix elements for the photoemission process from the adsorbate.[47]

2. Momentum matrix element

The momentum matrix element $\vec{P}_{if}$ which appears in Eq. (4) is a complex vector which, in general, will depend on the initial and final states under investigation; especially, it will be, in general, a function of the magnitude and direction of the wave vector of the emitted photoelectron.

The study of the momentum matrix element by angle-dependent photoemission is potentially powerful because it gives information on the wave functions of the states involved and their symmetry character.[48] Because in our setup the photoelectron emission angle changes, the corresponding change in $\vec{P}_{if}$ has to be considered. Basic insight into the functional behavior of $\vec{P}_{if}$ can be gained from considerations of localized core level states of oriented atoms. Here, $\vec{P}_{if}$ can be explicitly written down as a function of the initial state quantum numbers (l,m), radial matrix elements for the $(l+1)$ and $(l-1)$ excitation channels, the corresponding partial wave scattering phase shifts due to the emission process, and the detection direction θ_D.[49] Already for this very simple case, rather complicated analytical expressions result.

In contrast to photoemission from single, localized core level states, a continuum of states defined by their band index and three-dimensional wave vector $\vec{k}$ has to be considered in the case of photoemission from valence bands. By using the picture of a linear combination of atomic orbitals (LCAOs), it is possible to express the valence band states as coherent combinations of basis states localized at the atoms of the crystal unit cell.[38] Writing the final state in the same basis set allows us, in principle, to calculate $\vec{P}_{if}$ [see Eq. (4)] and to gain insight into the angular distributions contributed by certain types of atomic orbitals. For the simplified case of emission from a single type of atomic orbital, the result is basically a product of the angular distribution caused by the single atomic orbital, which is then modified by a photoemission structure factor describing interference caused by the periodic arrangement of this atomic orbital.[50]

These interference effects due to the plane wave part in the initial and final state wave functions will be dominating if we switch from the LCAO view to the 2-OPW nearly-free-electron model. As shown in Ref. 37, $\vec{P}_{if}$ will be a constant vector pointing into the direction of the reciprocal lattice vector $\vec{G}$ involved in the generation of the NFE bands:

$$\vec{P}_{if} \propto \vec{G}(V_G/\hbar\omega). \tag{11}$$

For our case, we can, thus, assume that the momentum matrix element will be directed in the direction of the surface normal, and the angular dependence of the A_z component of the electric field in the sample will be a determining factor of the overall angular dependence of the photoemitted intensity under p-polarized excitation.

The 2-OPW model expression, however, clearly is valid only in a limited region of $\vec{k}$ space. An increasing number of plane wave components will be necessary to describe an extended region of the band structure. The direction and magnitude of $\vec{P}_{if}$ will then be determined by the respective wave vectors and pseudopotential components of the initial and final states in a more complicated but straightforward way.[11]

To summarize, from the various angle-dependent factors discussed above, the following simple model for the photoemitted angle-dependent intensities in our experimental setup emerges:

$$I_{if}^{nPPE} \propto |A_z(\theta_i, \epsilon) \cdot P_z|^{2n}. \tag{12}$$

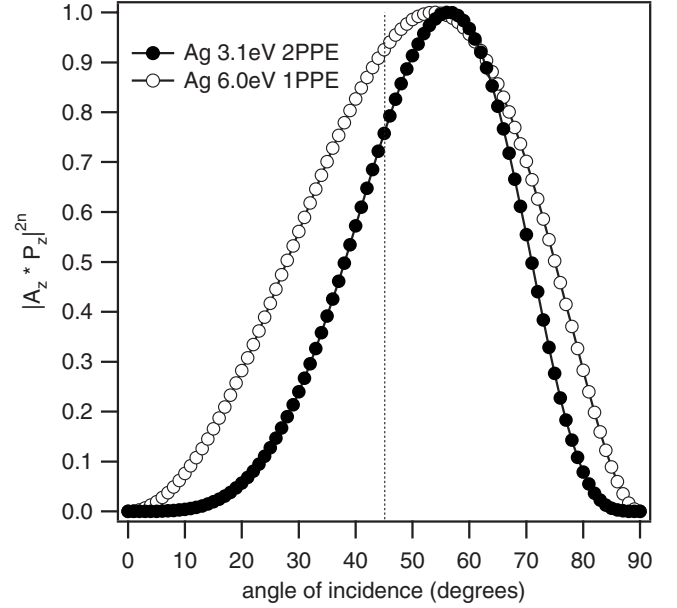In Fig. 6, we show how the angular dependence of the A_z

FIG. 6. Relative variation of the intensity factor $|A_zP_z|^{2n}$ for nPPE from silver assuming constant P_z and considering only effects due to the changing angle of incidence.

components shown in Fig. 5 translates to the photoemitted intensity by looking at the square (1PPE) or the fourth power (2PPE) of A_z. Due to the higher nonlinearity, a sharper and more asymmetric distribution with respect to detection relative to the surface normal at 45° is expected for 2PPE.

IV. RESULTS AND DISCUSSION

We will first discuss the results relevant to the observed dispersion of the sp-band transition peak and then go on to analyze the observed intensity variation.

A. Dispersion of the observed transitions

We have calculated the theoretically expected dispersion for a 2-OPW nearly-free-electron band structure of the sp bands near the Γ-L direction using a value of $E_{gap}=2V_{111}=4.2$ eV,[9,10] the perpendicular component of the reciprocal lattice vector $\vec{G}(\bar{1},\bar{1},\bar{1})=g_z=-2\pi/2.36$ Å, and a variable inner potential of V_0. The optical transitions and the observed angles outside the sample have been determined for the transition energies of 6.0 and 6.2 eV, corresponding to 1PPE and 2PPE, respectively.

To estimate the influence of the bias voltage on the observed parallel component of k, we have also measured the dispersion of the surface state and found effective masses of $m_{eff}=0.3$. This is slightly less than the published values of $m_{eff}=0.40$ (Ref. 20) or $m_{eff}=0.45$,[19] and means that we will observe an apparently increased dispersion of the sp-band transition with angle, which, in turn, leads to an inner potential which is systematically too low. A large inner potential has the effect to limit the k space which is accessible and, thus, would reduce the observed dispersion.

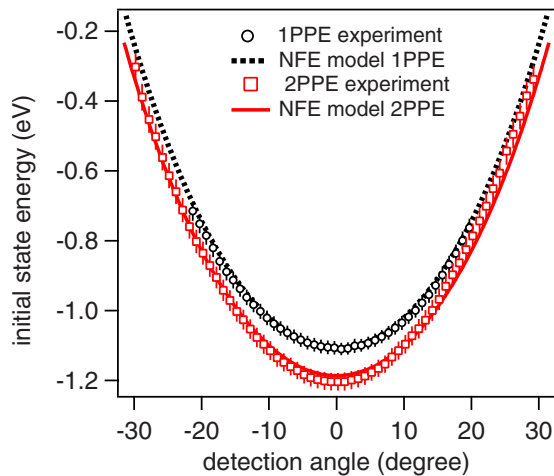The obtained theoretical angular dispersions of the sp-band transition are compared to the experimental ones in

FIG. 7. (Color online) Comparison of the experimentally measured and calculated dispersions from a 2-OPW nearly-free-electron model for the *sp*-band transition on Ag(111) by 1PPE ($\hbar\omega$ =6.0 eV) and 2PPE ($\hbar\omega$=6.2 eV).

Fig. 7. Our model only slightly underestimates the change in apparent binding energy at normal emission when going from 6.0 to 6.2 eV photon energy. This should be considered as a reliable measure of the degree of agreement with the assumed band-structure model because the dispersion with energy at normal emission is not influenced by electron refraction. The binding energy changes by approximately 0.1 eV, which is half the effective photon energy change of 0.2 eV. This behavior is caused by the dispersion of both the initial and final *sp*-band states, and the observed value agrees with previous studies.[28,31]

Good agreement is also obtained for the angular dispersion, considering the simplicity of the model we applied. However, in addition to the dispersion caused by the change in the observed direct transition in $\vec{k}$ space, the change of the peak position observed in the spectrum will be governed to a large extent by refraction. Refraction is strong because the potential step V_R [Eq. (1)] that has to be overcome at the surface is of nearly the same size as the energy of the photoelectron inside the material. This means that the influence of the potential step has to be known sufficiently well to still allow insight into the band structure of the sample by using very low energy photoelectrons. We find the best agreement with values of the inner potential $V_0=V_R-\Phi=2$ eV when neglecting the effect of the bias voltage and of $V_0=5$ eV when assuming that the relative change in the parallel component of k is roughly similar to the value observed for the surface state relative to the published values. In previous ARPES studies, inner potentials V_0 of 4 eV,[14] 5 eV,[13] and 6.7 eV (Ref. [51]) (defined with respect to the Fermi level) have been used. This compares quite well with our value. It has to be noted, however, that in most ARPES studies, the inner potential is mainly used to fix the position of the free electron final state, and then to infer from this the initial state dispersion in synchrotron experiments with varying photon energy and electron detection along the surface normal, which avoids refraction effects. Also, because of the higher photon energies in ARPES experiments, the refraction effects
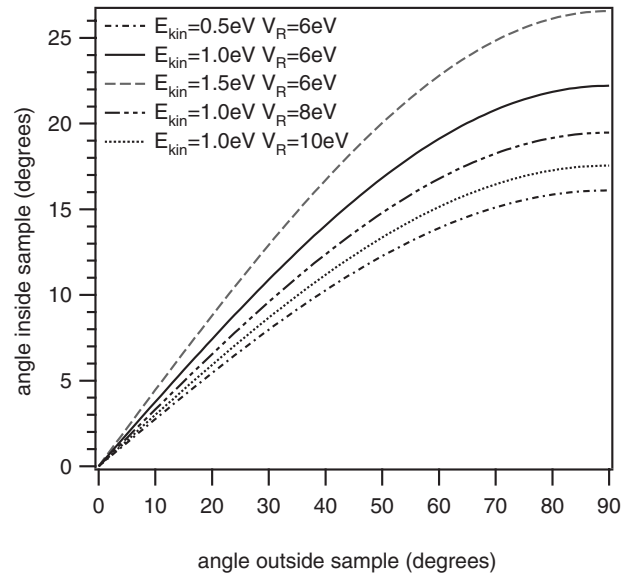

FIG. 8. Refraction of photoelectrons limits the range of angles inside the sample which can be sampled outside. Calculations according to Eq. (1). Electrons which are detected at angles up to ±30° originate from a cone of typically 10° or less in our experimental setup.

are still comparatively less significant even at off-normal detection.

In a realistic band structure, one and the same parameter does not describe the final state band structure and the refraction effect at the same time. Also, the inner potential is known to be energy dependent from LEED studies.[52] Taking all this into account, there is considerable uncertainty about the exact value of the potential step that causes refraction, especially at the very low energies involved in 2PPE experiment. In the ARPES experiments, a spread of nearly 3 eV in V_0 is seen in the different studies. While this variation might be insignificant for band mapping in ARPES experiments at high photon energies, the error in the outside angles introduced at low electron energies will overwhelm the effects caused by the band structure, because much of the observed dispersion can be adjusted by simply assuming a different inner potential V_0. If we reverse the assumptions realizing that the *sp*-band structure is sufficiently well known from ARPES studies with high energy photons, we have a sensitive probe of the inner potential in the form of the very low energy photoelectrons with a known initial *k*-space distribution before the refraction. In this sense, the well-defined *sp*-band transition could serve as a calibration against which to measure the inner potential effects.

The knowledge of the inner potential is crucial for the interpretation of spectroscopic and imaging techniques which involve low-energy electrons,[34] for instance, low-energy electron microscopy and photoemission electron microscopy. Furthermore, the effective potential at very low energies is influenced to a large extent by exchange and correlation effects,[34] and as only a few methods exist for the measurement of the surface potential step,[53] the analysis of low-energy photoelectrons could provide additional insight about the importance of these interactions.

As we show in Fig. 8, all electrons detected in vacuum will originate from a cone with half opening angle near 10° inside the sample for the kinetic energies employed in our experiment. This will effectively mean that the sensed region of reciprocal space is reduced considerably, and along with this, the sensitivity to any change in the momentum matrix element $\vec{P}_{if}$. This does not mean, however, that bulk band mapping by angle-dependent 2PPE is generally impossible. Let us assume that typically the largest kinetic energies in 2PPE experiments can be of the order of the work function, e.g., $E_{kin}=4$ eV, then taking $V_R \approx 8$ eV and a maximum outside detection angle of $\theta_D=70°$, one arrives at internal angles θ_{int} of approximately 30°, which translate to a parallel k component $k_{\parallel}^{max}=\sqrt{(2m/\hbar^2)(E_{kin}+V_R)(1-\cos^2 \theta_{int})}=0.88$ Å^{-1}, which is of the order of the Brillouin zone dimension. Thus, significant information about the dispersion of the parallel wave vector components can be obtained in principle.

To summarize, on one hand, the low energy of the observed electrons is clearly a severe practical limitation for their application to map electronic band structure if the refraction cannot be taken into account quantitatively. On the other hand, if we assume that the *sp*-band structure is known sufficiently well, we have a sensitive probe of the inner potential.

B. Intensities

Because of the inherent asymmetry in the experimental setup, for both 1PPE and 2PPE, an asymmetric angular intensity distribution is expected. Because the incident angle θ_i is changed asymmetrically with respect to the surface normal, all other factors depending on the incidence angle are expected more or less to also show this asymmetry. This can be seen in Fig. 6. Both the 1PPE and 2PPE distributions should be clearly asymmetric with respect to the surface normal, and the 2PPE intensity should be narrower. The 1PPE intensity that we observe (Fig. 3), however, does not fit the simple Fresnel model. Instead, we suggest that, in this case, we see the influence of surface photoemission. This is supported by 1PPE measurements on Cu(001), where we observe excellent agreement with the Fresnel model.

We have simulated the photoemitted intensities as a function of the detection angle for the case of 1PPE and 2PPE according to the model of Eq. (12). For the dielectric function of silver, we used the values of $\epsilon=(n+ik)^2$, with $(n+ik)=0.05+2.275i$ ($\hbar\omega=3.1$ eV) and $(n+ik)=1.18+1.312i$ ($\hbar\omega=6.0$ eV).[54] For the dielectric function of copper, we used the values of $(n+ik)=1.32+2.12i$ ($\hbar\omega=3.1$ eV) and $(n+ik)=1.01+1.60i$ ($\hbar\omega=6.0$ eV),[54] with the final result not very sensitively depending on the exact value of all of these parameters.

The peaks of the *sp*-band transitions in the experimental photoemission spectra were fitted to Gaussians on a linear background, and from this fit, the intensity in the peak was obtained. The results are shown in Fig. 9. Very good agreement is found assuming an effective momentum matrix element pointing along the surface normal and having a constant magnitude. This is in agreement with the expectation from the 2-OPW NFE model, where $\vec{P}_{if}$ will be constant and
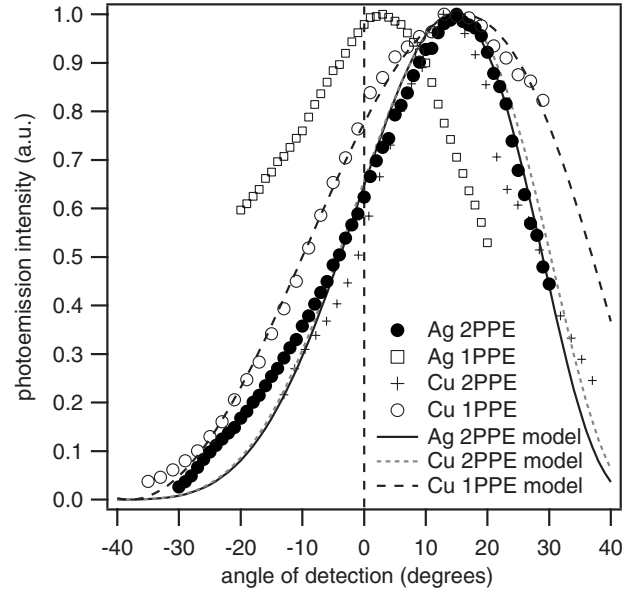

FIG. 9. Comparison of experimentally measured and simulated intensities in the *sp*-band transition on Ag(111) by 2PPE and 1PPE, and measured and simulated intensities for 2PPE and 1PPE from electrons with initial states at the Fermi energy of Cu(001). The expected distribution for 1PPE from Ag(111) according to the Fresnel model corresponds closely to the model curve shown for 1PPE from Cu(001). For both experiments, $\hbar\omega=3.1$ eV for 2PPE and $\hbar\omega=6.0$ eV for 1PPE.

point in the direction of $\vec{G}=(1,1,1)$. The agreement of the experimental data of Ag(111) is not as good at negative exit angles, which we attribute mainly to the uncertainty in extracting low peak intensities on an unknown background (note the very low intensity at negative angles in Fig. 3).

As can be seen in Fig. 9, the experimental intensities in 1PPE from Ag(111) do not fit the expected behavior of Fig. 6. To motivate why we think that this behavior is anomalous, we apply our model to a different substrate, Cu(001). So far, the only assumptions we have made for the analysis of the angle-dependent intensity on Ag(111) is that P_{if} is constant and points along the z axis. We also showed that the A_z component of the electric field at the surface shows a universal angle-dependent change with incidence angle. Thus, the intensity variation that we have observed in 2PPE on Ag(111) should be quite generally valid for transitions which are governed by this field component, also on different substrates. This is why we choose to compare in Fig. 9 the data measured on Cu(001). The intensity data were obtained for initial state electrons near the Fermi energy. For these electrons originating from the Cu *sp* band (Δ_1 symmetry), the optical selection rules for fcc surfaces (Δ_1 final state) dictate that again the A_z component is the most relevant near normal emission. So we should have a comparable intensity variation as on Ag(111). Figure 9 shows that this is indeed the case for the 2PPE measurements on Cu(001) and, moreover, that the 1PPE data from Cu(001) shows the expected broader intensity distribution with a pronounced asymmetry, in contrast to what is observed for 1PPE on Ag(111).
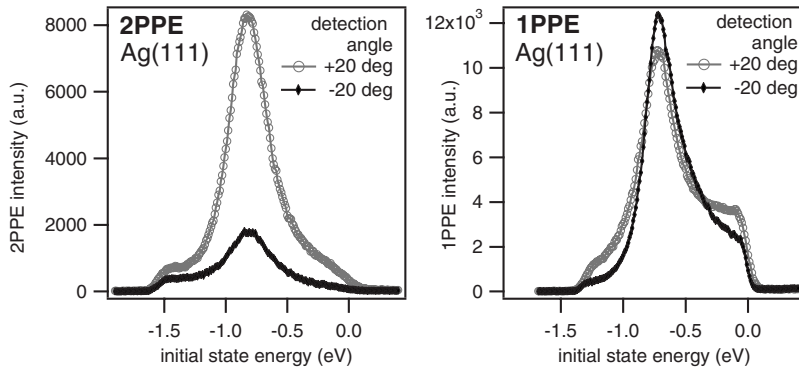
FIG. 10. Comparison of 1PPE and 2PPE spectra for detection angles symmetrically ±20° to the surface normal. The 1PPE spectra show the influence of surface photoemission, indicated by a very asymmetric peak shape and large background.

To analyze the 1PPE data further, we show in Fig. 10 1PPE and 2PPE spectra taken from Ag(111) (data from Fig. 3) at detection angles of ±20° to the surface normal. Firstly, one immediately notes the much more asymmetric peak shape of the 1PPE spectra as compared to a rather symmetric 2PPE peak. Secondly, the peak intensity relative to the background clearly shows an anomalous behavior for 1PPE. Whereas for 2PPE both peak height and background are increased at positive angles (larger A_z component), the 1PPE spectra show a larger background at positive angles, but with a reduced peak height. Both these observations point to the influence of surface photoemission. It has been shown previously that surface photoemission causes a very asymmetric peak shape for the sp-band transition on Ag(111).[25,26] This asymmetry is created by additional photoemission due to transitions that do not need to conserve crystal momentum and which show up as a broad background in the spectrum. These transitions involve an increased range of k vectors different from the ones determined by crystal momentum conservation in the bulk sp-band transition. Our observations are also consistent with the fact that we observe an increased influence of surface photoemission at angles where the A_z component and also its change at the surface become larger according to Eq. (8). Because the surface photoemission is an alternative coherent pathway for photoemission, the surface and bulk photoemission channels interfere, modifying the intensity and asymmetry of the bulk transition peak. This is observed as the reduced peak height of the 1PPE transition as compared to an increased background. As is shown in Eq. (7), one can try to model the influence of surface photoemission by an additional complex fit parameter C_S in the transition matrix element, by which the interference between surface and bulk photoemissions is phenomenologically simulated. While we can obtain very good agreement with the measured data for a specific choice of C_S (not shown), the measured angular range of 1PPE spectra does not allow a final conclusion about the physical significance of this approach. Additionally, one should expect that the interference effects will be a function of the position of the sp-band peak in the spectrum, and thus, an energy-independent C_S might not be sufficient. This is why we limited ourselves to demonstrate that in agreement with previous studies, surface photoemission seems to have an appreciable angle-dependent effect also in our 1PPE measurements. In contrast, it has been shown previously that the 2PPE spectra can be simulated without taking into account surface photoemission.[33]

This is consistent with our measurements.

Our observations are relevant in a further context. The Fresnel equations neglect the nonlocal influences on the electromagnetic field at the surface that would have to be described via a dielectric function $\epsilon(\vec{q}, \omega)$ that not only depends on the frequency ω but also on the wave vector $\vec{q}$.[55,56] These effects are most pronounced near the plasmon energy, and lead to characteristic changes in the A_z component of the field in the first few angstroms of the surface. Because we were observing a bulk transition, the sensitivity to such optical effects intrinsic to the presence of a surface should be diminished. It is interesting to note, however, that such effects might be within reach of comparative 2PPE and 1PPE experiments. For instance, the plasmon resonance of silver is at 3.8 eV,[57] an energy which can be bracketed by common double- and single-photon energies to possibly acquire photoemission data which are more or less strongly influenced by nonlocal effects.[58] In this context, the observation that surface photoemission is unimportant in 2PPE with single-photon energies below the plasmon energy, but visible in 1PPE with a photon energy above the plasmon threshold, could be important.

V. SUMMARY

We have shown that the observed dispersion of the sp-band transition on Ag(111) in 1PPE and 2PPE can be analyzed using a nearly-free-electron model for the initial and final states involved. The observed dispersion agrees with the known band structure. To gain exact band-structure information, the strong refraction of the low-energy electrons needs to be taken into account quantitatively. This is limited by the degree to which the inner potential is known. We suggest using the low-energy photoelectrons from the sp-band transition as a probe for the potential step at the surface. The observed intensity distributions in 2PPE from Ag(111) can be well described by a phenomenological model which employs the Fresnel equations to calculate the electric field components inside the sample. Very good agreement is found using known optical constants and a momentum matrix element which is directed into the direction of the surface normal. By comparison to Cu(001), we have shown that the observed intensity distributions for 1PPE and 2PPE are

valid for this orientation of the momentum matrix element, and surface photoemission can be neglected. In contrast, the observed intensity distribution for one-photon photoemission from Ag(111) does not fit the simple Fresnel model. We interpret this as the influence of surface photoemission. With the mentioned limitations in mind, our study shows that relevant information about the electronic structure at surfaces can be obtained with angle-dependent 2PPE measurements.

*petek@pitt.edu

[1] S. Hüfner, *Photoelectron Spectroscopy* (Springer Verlag, Berlin, 1995).

[2] J. K. Grepstad and B. J. Slagsvold, Solid State Commun. **34**, 821 (1980).

[3] P. Aebi, J. Osterwalder, R. Fasel, D. Naumovic, and L. Schlapbach, Surf. Sci. **307-309**, 917 (1994).

[4] J. Braun, Rep. Prog. Phys. **59**, 1267 (1996).

[5] R. Haight, Surf. Sci. Rep. **21**, 275 (1995).

[6] H. Petek and S. Ogawa, Prog. Surf. Sci. **56**, 239 (1997).

[7] S. Ogawa, H. Nagano, and H. Petek, Phys. Rev. B **55**, 10869 (1997).

[8] P. S. Wehner, R. S. Williams, S. D. Kevan, D. Denley, and D. A. Shirley, Phys. Rev. B **19**, 6164 (1979).

[9] J. G. Nelson, S. Kim, W. J. Gignac, R. S. Williams, J. G. Tobin, S. W. Robey, and D. A. Shirley, Phys. Rev. B **32**, 3465 (1985).

[10] M. A. Mueller, A. Samsavar, T. Miller, and T.-C. Chiang, Phys. Rev. B **40**, 5845 (1989).

[11] H. Becker, E. Dietz, U. Gerhardt, and H. Angermüller, Phys. Rev. B **12**, 2084 (1975).

[12] D. J. Spanjaard, D. W. Jepsen, and P. M. Marcus, Phys. Rev. B **15**, 1728 (1977).

[13] S. C. Wu, H. Li, J. Sokolov, J. Quinn, Y. S. Li, and F. Jona, J. Phys.: Condens. Matter **1**, 7471 (1989).

[14] H. Wern, R. Courths, G. Leschik, and S. Hüfner, Z. Phys. B: Condens. Matter **60**, 293 (1985).

[15] E. Tamura, R. Feder, B. Vogt, B. Schmiedeskamp, and U. Heinzmann, Z. Phys. B: Condens. Matter **77**, 129 (1989).

[16] P. Heimann, H. Neddermeyer, and H. F. Roloff, J. Phys. C **10**, L17 (1977).

[17] H. F. Roloff and H. Neddermeyer, Solid State Commun. **21**, 561 (1977).

[18] T. C. Hsieh, P. John, T. Miller, and T.-C. Chiang, Phys. Rev. B **35**, 3728 (1987).

[19] R. Paniago, R. Matzdorf, G. Meister, and A. Goldmann, Surf. Sci. **336**, 113 (1995).

[20] G. Nicolay, F. Reinert, S. Schmidt, D. Ehm, P. Steiner, and S. Hüfner, Phys. Rev. B **62**, 1631 (2000).

[21] N. E. Christensen, Phys. Status Solidi B **54**, 551 (1972).

[22] O. Jepsen, D. Glötzel, and A. R. Mackintosh, Phys. Rev. B **23**, 2684 (1981).

[23] H. Eckardt, L. Fritsche, and J. Noffke, J. Phys. F: Met. Phys. **14**, 97 (1984).

[24] G. Panaccione, G. Cautero, M. Cautero, A. Fondacaro, M. Grioni, P. Lacovig, G. Monaco, F. Offi, G. Paolicelli, M. Sacchi, N. Stojic, G. Stefani, R. Tommasini, and P. Torelli, J. Phys.: Condens. Matter **17**, 2671 (2005).

[25] T. Miller, W. E. McMahon, and T.-C. Chiang, Phys. Rev. Lett. **77**, 1167 (1996).

[26] T. Miller, E. D. Hansen, W. E. McMahon, and T. C. Chiang, Surf. Sci. **376**, 32 (1997).

[27] S. R. Barman, C. Biswas, and K. Horn, Phys. Rev. B **69**, 045413 (2004).

[28] K. Giesen, F. Hage, F. J. Himpsel, H. J. Riess, and W. Steinmann, Phys. Rev. Lett. **55**, 300 (1985).

[29] R. W. Schoenlein, J. G. Fujimoto, G. L. Eesley, and T. W. Capehart, Phys. Rev. B **43**, 4688 (1991).

[30] R. L. Lingle, N. H. Ge, R. E. Jordan, J. D. McNeill, and C. B. Harris, Chem. Phys. **205**, 191 (1996).

[31] S. Pawlik, R. Burgermeister, M. Bauer, and M. Aeschlimann, Surf. Sci. **402-404**, 556 (1998).

[32] V. M. Shalaev, C. Douketis, T. Haslett, T. Stuckless, and M. Moskovits, Phys. Rev. B **53**, 11193 (1996).

[33] N. Pontius, V. Sametoglu, and H. Petek, Phys. Rev. B **72**, 115105 (2005).

[34] D. K. Saldin and J. C. H. Spence, Ultramicroscopy **55**, 397 (1994).

[35] R. Courths and S. Hüfner, Phys. Rep. **112**, 53 (1984).

[36] R. Y. Koyama and N. V. Smith, Phys. Rev. B **2**, 3049 (1970).

[37] A. I. Golovashkin, A. I. Kopeliovich, and G. P. Motulevich, Sov. Phys. JETP **26**, 1161 (1968).

[38] W. Schattke, M. A. Van Hove, F. J. Garcia de Abajo, R. Diez Muino, and N. Mannella, *Solid-State Photoemission and Related Methods: Theory and Experiment* (Wiley-VCH, 2003), pp. 50–115.

[39] R. Loudon, *The Quantum Theory of Light* (Oxford University Press, New York, 2000).

[40] H. Ueba and B. Gumhalter, Prog. Surf. Sci. **82**, 193 (2007).

[41] M. V. Klein and T. E. Furtak, *Optics* (Wiley, New York, 1986).

[42] A. Damascelli, G. Gabetta, A. Lumachi, L. Fini, and F. Parmigiani, Phys. Rev. B **54**, 6031 (1996).

[43] F. Pforte, T. Michalke, A. Gerlach, A. Goldmann, and R. Matzdorf, Phys. Rev. B **63**, 115405 (2001).

[44] P. J. Feibelman, Surf. Sci. **46**, 558 (1974).

[45] M. A. B. Whitaker, J. Phys. C **11**, L151 (1978).

[46] Y. J. Chabal, Surf. Sci. Rep. **8**, 211 (1988).

[47] L. Gundlach, J. Szarko, L. D. Socaciu-Siebert, A. Neubauer, R. Ernstorfer, and F. Willig, Phys. Rev. B **75**, 125320 (2007).

[48] F. Pforte, A. Gerlach, A. Goldmann, R. Matzdorf, J. Braun, and A. Postnikov, Phys. Rev. B **63**, 165405 (2001).

[49] S. M. Goldberg, C. S. Fadley, and S. Kono, J. Electron Spectrosc. Relat. Phenom. **21**, 285 (1981).

[50] H. Daimon and F. Matsui, Prog. Surf. Sci. **81**, 367 (2006).

[51] A. Samsavar, T. Miller, and T. C. Chiang, J. Phys.: Condens.

Matter **2**, 1141 (1990).

[52] S. Walter, V. Blum, L. Hammer, S. Muller, K. Heinz, and M. Giesen, Surf. Sci. **458**, 155 (2000).

[53] J. C. H. Spence, H. C. Poon, and D. K. Saldin, Microsc. Microanal. **10**, 128 (2004).

[54] P. B. Johnson and R. W. Christy, Phys. Rev. B **6**, 4370 (1972).

[55] K. L. Kliewer, Surf. Sci. **101**, 57 (1980).

[56] P. J. Feibelman, Prog. Surf. Sci. **12**, 287 (1982).

[57] S. Suto, K.-D. Tsuei, E. W. Plummer, and E. Burstein, Phys. Rev. Lett. **63**, 2590 (1989).

[58] A. Liebsch and W. L. Schaich, Phys. Rev. B **52**, 14219 (1995).